Magnetic Resonance in Medicine

A size-adaptive 32-channel array coil for awake infant neuroimaging at 3 Tesla MRI

Anpreet Ghotra[1] | Heather L. Kosakowski[2] | Atsushi Takahashi[2] |
Robin Etzel[1] | Markus W. May[1] | Alina Scholz[1] | Andreas Jansen[3,4] |
Lawrence L. Wald[5,6] | Nancy Kanwisher[2] | Rebecca Saxe[2] | Boris Keil[1,4]

[1]Institute of Medical Physics and Radiation Protection, Department of Life Science Engineering, TH Mittelhessen University of Applied Sciences, Giessen, Germany

[2]Department of Brain and Cognitive Sciences and McGovern Institute, Massachusetts Institute of Technology, Cambridge, MA, USA

[3]Department of Psychiatry and Psychotherapy, University of Marburg, Marburg, Germany

[4]Center for Mind, Brain and Behavior (CMBB), Marburg, Germany

[5]Athinoula A. Martinos Center for Biomedical Imaging, Department of Radiology, Harvard Medical School, Massachusetts General Hospital, Charlestown, MA, USA

[6]Harvard-MIT Division of Health Sciences and Technology, Cambridge, MA, USA

Correspondence
Anpreet Ghotra, Institute of Medical Physics and Radiation Protection, TH Mittelhessen University of Applied Sciences, Giessen 35390, Germany.
Email: anpreet.ghotra@lse.thm.de

Funding information
MINT Foundation; MIT

Purpose: Functional magnetic resonance imaging (fMRI) during infancy poses challenges due to practical, methodological, and analytical considerations. The aim of this study was to implement a hardware-related approach to increase subject compliance for fMRI involving awake infants. To accomplish this, we designed, constructed, and evaluated an adaptive 32-channel array coil.

Methods: To allow imaging with a close-fitting head array coil for infants aged 1-18 months, an adjustable head coil concept was developed. The coil setup facilitates a half-seated scanning position to improve the infant's overall scan compliance. Earmuff compartments are integrated directly into the coil housing to enable the usage of sound protection without losing a snug fit of the coil around the infant's head. The constructed array coil was evaluated from phantom data using bench-level metrics, signal-to-noise ratio (SNR) performances, and accelerated imaging capabilities for both in-plane and simultaneous multislice (SMS) reconstruction methodologies. Furthermore, preliminary fMRI data were acquired to evaluate the in vivo coil performance.

Results: Phantom data showed a 2.7-fold SNR increase on average when compared with a commercially available 32-channel head coil. At the center and periphery regions of the infant head phantom, the SNR gains were measured to be 1.25-fold and 3-fold, respectively. The infant coil further showed favorable encoding capabilities for undersampled k-space reconstruction methods and SMS techniques.

Conclusions: An infant-friendly head coil array was developed to improve sensitivity, spatial resolution, accelerated encoding, motion insensitivity, and subject tolerance in pediatric MRI. The adaptive 32-channel array coil is well-suited for fMRI acquisitions in awake infants.

KEYWORDS

accelerated MRI, magnetic resonance imaging, neonatal imaging, pediatric imaging, pediatric MRI coil, phased array coil

1 | INTRODUCTION

Functional magnetic resonance imaging (fMRI) has proven valuable to noninvasively characterize adult brain functions over the last 25 years. Recently, substantial effort has been made to bring fMRI to the pediatric population, and it has already given great insight into the maturational processes that take place after birth across multiple fields of inquiry. Applications of fMRI with infants and toddlers have become a rapidly expanding field of research. However, the use of MRI during infancy and toddlerhood remains a challenging undertaking due to practical, methodological, and analytical problems that arise when imaging this young population.

While early pediatric functional brain imaging studies were conducted using sedation and anesthesia,[1] over the last 15 years, many fMRI scans with infants have been carried out during natural sleep.[2-4] Implementing task-based fMRI with awake infants poses challenges regarding infant handling, motion reduction, and subject compliance. Nevertheless, obtaining high-quality functional images from awake infants provides precise details about the early development of human perception, cognition, and behavior.[5,6]

After the first months of birth, brain development is characterized by rapid growth. In particular, the gray matter volume expands 106% in the first year,[7] and in total, the neonate's average head circumference increases from 35 to 43 cm during the first 6 months, reaching 46 cm at the end of the first year.[8] This early period is also crucial in brain development, as axonal-dendritic connections are formed, followed by myelination and neuronal specification.[9] However, postnatal brain plasticity is also associated with increased vulnerability to developing errors in normal orchestration, neuronal connectivity, and the integration of neuronal activity.

The rapid changes in head sizes raise a major concern when it comes to obtaining optimum signal reception in infant brain MRI applications during early life, where a close-fitting coil helmet design is critical to gain maximum sensitivity from high-density coil arrays. One way of achieving this goal is to use customized head coils for infants[4] or even a set of differently sized head array coils to enable use of MRI for a wider range of the pediatric population while maintaining a snug fit of the coil to the subject's head.[10] However, the latter coil concept involves some inconveniences in terms of costs and workflow. Another solution in providing close-fitting detector design is employing an arrangement of freely adjustable coil elements.[11] Nevertheless, with the need for large coil counts, this solution has some practical implications and requires substantial technical efforts in terms of geometric fixation.

A major consideration for tightly fitting coil helmets is the limitation in using conventional MRI sound protection gear for attenuating the scanner's acoustic noise. To address this, researchers use thin pediatric earmuff pads, which compromise sound attenuation, and thus, reduce the subject's overall tolerance in completing an MRI scan.

Given the small market volume for pediatric imaging, none of the commercial vendors provide state-of-the-art pediatric-sized head coils exceeding 16 channels. Therefore, both clinical and research institutions often use adult head coils when conducting pediatric brain MRI. This renders the brain suboptimal in terms of sensitivity reception and encoding capabilities for accelerated imaging. In addition, the infant's anatomy of a short neck raises difficulties in placing the subject's head at the isocenter of the adult head coil with the shoulders touching the lower end of the head coil; this prevents the infant's head from fully entering the coil.

Multiple aspects of the coil array must be addressed to bring task-based infant neuro-fMRI to the next level of sensitivity, spatial resolution, accelerated encoding, motion insensitivity, and subject tolerance. In the present work, the concept of an adjustable coil array is explored for awake infant brain imaging. We exploit the improved SNR and parallelism to accelerate image encoding, minimizing the total acquisition time and providing flexibility to collect a larger number of shorter scans.

2 | METHODS

2.1 | Coil design and construction

The 32-channel pediatric head coil was developed to accommodate head sizes for infants aged 1-18 months. Thus, a substantial and integral part of our coil design was the

identification and implementation of the optimal coil helmet. While circumference statistics as a function of age are well documented,[8,12,13] there is no source of 3-dimensional (3D) head-form shapes for infants of different age groups. Therefore, our modular coil former is based on the surface contours of aligned 3D MRI pediatric head scans from 20 groups of age-matched 1-, 6-, 12-, and 18-month-old infants. Each computed average age-matched head model was scaled to the 95th percentile of the statistical corresponding head circumferences.[8]

Following the concept of "one-size-fits-all," we implemented a coil helmet design with 3 anatomical-shaped independent coil segments (Figure 1). We used a computer-aided design (CAD) software (Rhino3D V.6.0, Robert McNeel & Associates, Seattle, WA, USA) to 3D model the array coil housing. The posterior part is integrated into the coil base so that the infant can be easily laid down without any other restrictive coil parts. After the infant is placed on the posterior coil part, 2 anterior coil segments can be laterally slid in around the infant's head. This mechanism allows continuous lateral coil-to-head adaption. In the anterior-posterior (AP) direction, the helmet can be adjusted in 4 increments of 5 mm each accommodating head sizes with AP diameters from 155 to 170 mm. This facilitates MR brain imaging of newborns to infants of approximately 18 months. In the most tightest helmet setting, the coil can accommodate infants with a head circumference of up to 44 cm, corresponding to an age of 6-7 months. For newborns up to 3 months, there is a small remaining space of approximately 1 to 1.5 cm between the infant's head and the coil former. For larger head sizes, ranging from 44 to 49 cm circumference, the coil helmet allows expansion in both the left-right and AP directions (Supporting Information Figures S1 and S2).

Instead of lying flat on the patient table, we designed the coil base as an inclined cradle seat to improve the subject's overall MRI scanning compliance. The cradle was designed to accommodate toddler of 18 months. For younger (and smaller) infants, cushions can be added to raise the lower cradle part, so that the infant's head comfortably accesses the head coil.
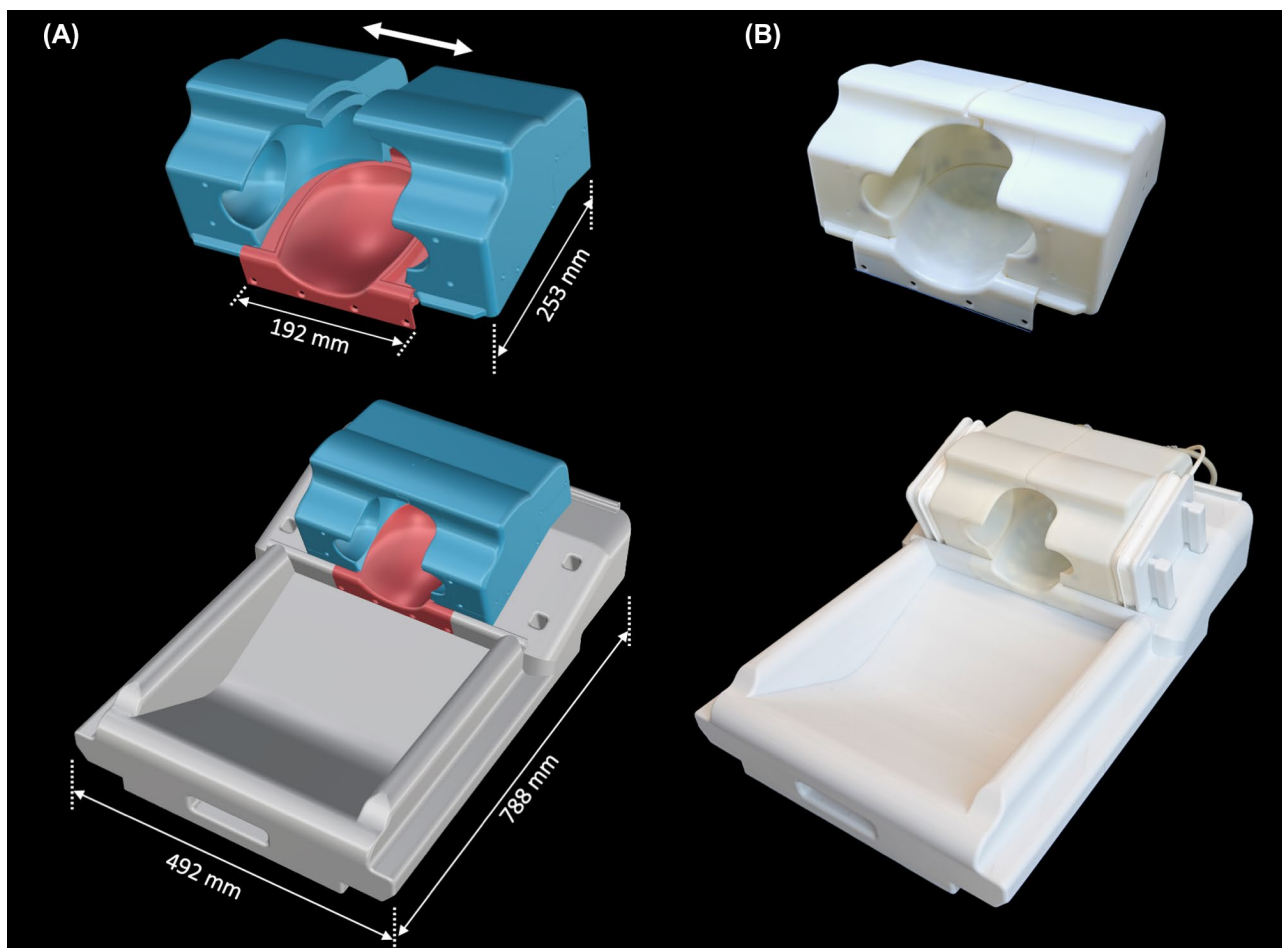
FIGURE 1 CAD design (A) and 3D printed model (B) of the adaptive array coil setup. The coil setup consists of an adjustable receiver array and an inclined cradle as a coil base. The posterior part (red) of the array coil is directly incorporated into the coil base, while the anterior parts (blue) allow adaptability to various infant head sizes (neonate to 18 months). Head immobilization is achieved using inflatable cushions, which are placed on the outer side of the anterior coil segments. The total weight of the infant coil amounts to 6.8 kg

FIGURE 2 Constructed and populated coil array. The posterior coil part (A) comprises 12 coil elements, and it is integrated into the housing base (B). The 2 anterior segments (C) consist of 10 elements each and are laterally adjustable for individual infant head sizes. Integrated earmuff compartments allow the usage of bulky sound attenuation gear while maintaining a snug fit of the lateral coil array segments

When incorporating high-density head array coils with a tight fit around the subject's head, the need to provide enough accomm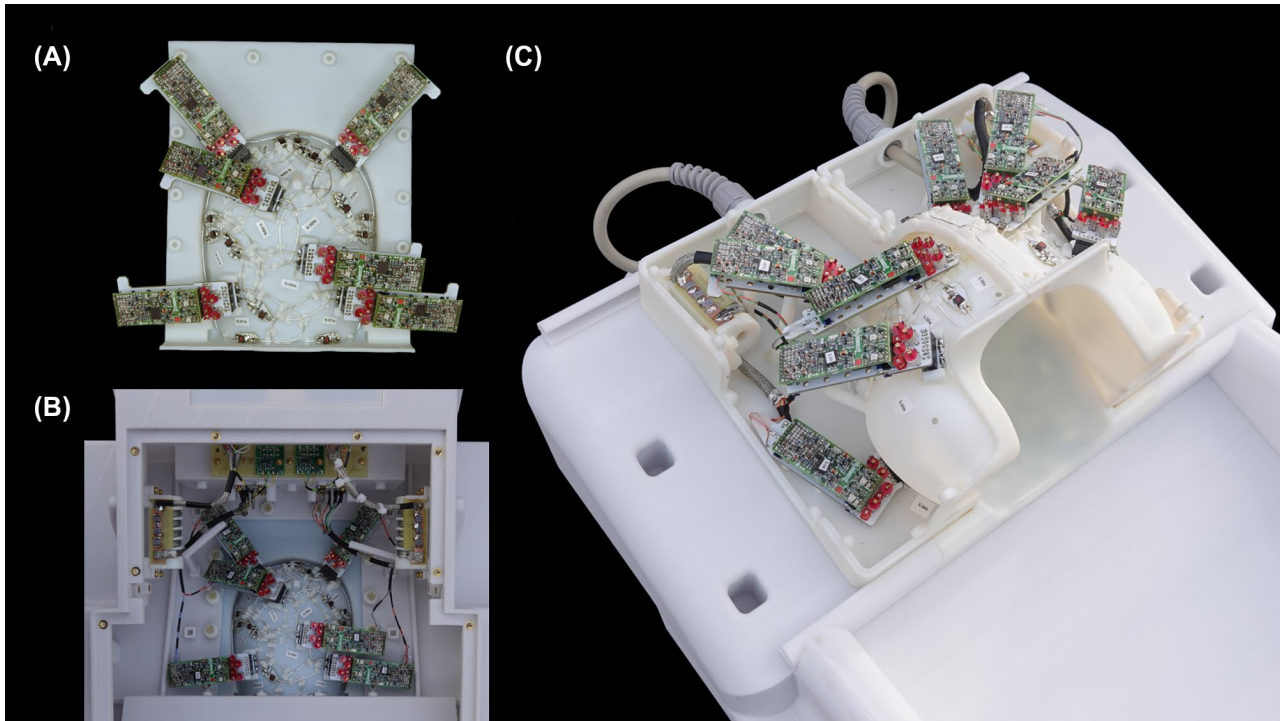odation for the subject's ear protection must be considered. Consequently, a critical design component was the implementation of dedicated earmuff compartments in both the right and left anterior coil housing sections. For further head immobilization, we placed inflatable cushions on the outer side of the anterior coil parts. This gentle pressure also seals the ear protection gear and reduces the infant head motion. We chose an open-faced coil topology without eye coil elements to prevent anxiety of participants and facilitate visual stimulation during task-based fMRI studies. All coil housing parts, including the covers and cradle, were 3D printed in polycarbonate (Fortus 360, Stratasys Ltd., Eden Prairie, MN, USA).

The optimum channel count for the constructed brain array was determined by the following: (a) the given geometrical constraints of the helmet, (b) the knowledge of the extent of anatomical coverage desired, and (c) the substantial loss of sample noise domination when going below a certain loop coil size. At 3 T MRI field strength, loop coil diameters of about 60 mm provide an unloaded-to-loaded Q-ratio of approximately 4, which is considered to be well sample noise dominated.[10]

Given the multiple constraints, a suitable element count for the developed coil former ranges from 30 to 34 channels. Recent advances in MR systems have ensured that nearly all 3-Tesla scanners currently installed utilize ≥ 32 receive channels. Therefore, we have implemented 32 loop elements into the constructed coil array.

We subdivided the total channel count into the posterior part with 12 elements, while the 2 anterior head parts house 10 elements each (Figure 2 and Supporting Information Figure S3). The majority of the loop elements were implemented with a diameter ranging from 58 to 67 mm. Some elements on the edges of the coil housing had to be shaped arbitrarily. The 2 larger loop elements surrounding the earmuff compartments comprise elliptical loop diameters of $d_1 = 85$ mm and $d_2 = 91$ mm. The array layout was established using critical overlap for direct neighboring element decoupling. This geometrically decoupled structure is also maintained when nearest neighbors are located in different coil part segments. Mechanically, this was achieved by incorporating an overlapping rim structure into the interconnecting areas of the housing parts, allowing the loops on separated sections to be geometrically decoupled.

2.2 | Electronics

Each loop element was constructed from a 1.2-mm thick silver-plated copper wire. The geometrical loop layout was implemented by small standoffs, integrated into the coil former design, in which the wires snapped into the desired position. We subdivided each wire loop element into 2 segments, between which a tuning capacitor C_{T1} was soldered.

On the opposite side, we incorporated a subconnector, where the preamplifier's daughterboard was mounted (Figure 3). The matching and detuning circuitry is placed on the front end of the preamplifier board rather than soldering those components directly onto the coil former. Therefore, the daughterboard contributes as a part of the coil circuit. The daughterboards were mechanically mounted on the helmet via 3D-printed plastic standoffs.

The coil's output network comprises a series variable capacitor C_M (GFX2700NM Sprague Goodman, Westbury, NY, USA) and a capacitive voltage divider (C_{TM}, C_{T2}) (Series 11, Knowles Capacitors, Norwich, UK), where C_{TM} contributes to both tuning and matching. C_{T2} forms with the inductance L and the PIN diode D the active detuning circuit, where C_{T2} and L are set to resonance when the PIN diode (MA4P4002B-402, Macom, Lowell, MA) is forward biased. Thus, a high impedance is inserted into the loop in series. This prevents current flow at Larmor frequency during transmission. In case the active detuning fails, we have incorporated a passive detuning circuit using a pair of cross-parallel passive diodes D_X (MADP-011048-TR3000, Macom, Lowell, MA, USA) with an additional series capacitor C_D. The latter blocks the active bias current but also tunes out the extra inductance resulting from the additional length of the copper trace. For a final safety feature, we have implemented a series fuse F (1999-6000-5700, current rating: 570 mA, Data Modul AG, Munich, Germany) for passive protection against large coil currents.

The fine adjustment of the resonance frequency was achieved by carefully controlling the variable tuning capacitor C_{T3}; the combination of C_M and C_{TM} matches the coil element's output under loaded conditions to a noise-matched impedance of 50 Ω. C_M and C_{TM} also provide the necessary impedance transformation for accomplishing preamplifier decoupling.[14] In this case, C_M transforms the preamplifier's input impedance to a parallel inductance across C_{TM}. Hence, this parallel LC circuit is set to resonance and introduces a high impedance in the coil loop (Supporting Information Figure S4). In this mode, minimal current flows in the loop, and inductive coupling to other coil elements are minimized. A twin preamplifier (Siemens Healthineers AG, Erlangen, Germany) was used to connect to a pair of adjacent coil elements. The preamplifier output cables within the 3 housing segments are bundled and passed through 3 cable traps to suppress common mode currents. The cable trap formers were 3D-printed, consist of 6 sinusoidal windings, and were tuned to Larmor resonant frequency using 3 series capacitors (33 pF, 39 pF, and 43 pF).

The 2 sliding anterior coil parts have separate plugs (ODU-MAC ZERO White Line, ODU GmbH & Co. KG, Mühldorf a. Inn, Germany), which connect to the posterior cradle base instead of directly to the scanner. The cradle base is then connected to the patient table using a sliding connection mechanism integrated into the coil housing. Consequently, the infant coil setup does not require any conventional coil plugs (Figure 4), which greatly optimizes imaging workflow conditions. This feature also facilitates the process of natural sleep studies, where the infant can be prepared and settled into sleep in a separate room and then placed onto the patient's scanner table with the entire coil setup.

FIGURE 3 Top: Loop coil element with its daughterboard and the developed dummy preamplifier board. The coil connects with a subconnector to the daughterboard, which comprises the output circuitry of the coil. Bottom: Corresponding circuit schematic of one coil element. Values for a 65-mm dia. loop element: $C_{T1} = 18\,\text{pF}$, $C_{T2} = 56\,\text{pF}$, $C_{T3} \approx 16\,\text{pF}$, $C_{TM} = 36\,\text{pF}$, $C_M \approx 24\,\text{pF}$, $C_D = 180\,\text{pF}$, $C_{RFC} = 1\,\text{nF}$, $L \approx 25\,\text{nH}$, $L_{RFC1} = L_{RFC2} = 2.7\,\mu\text{H}$
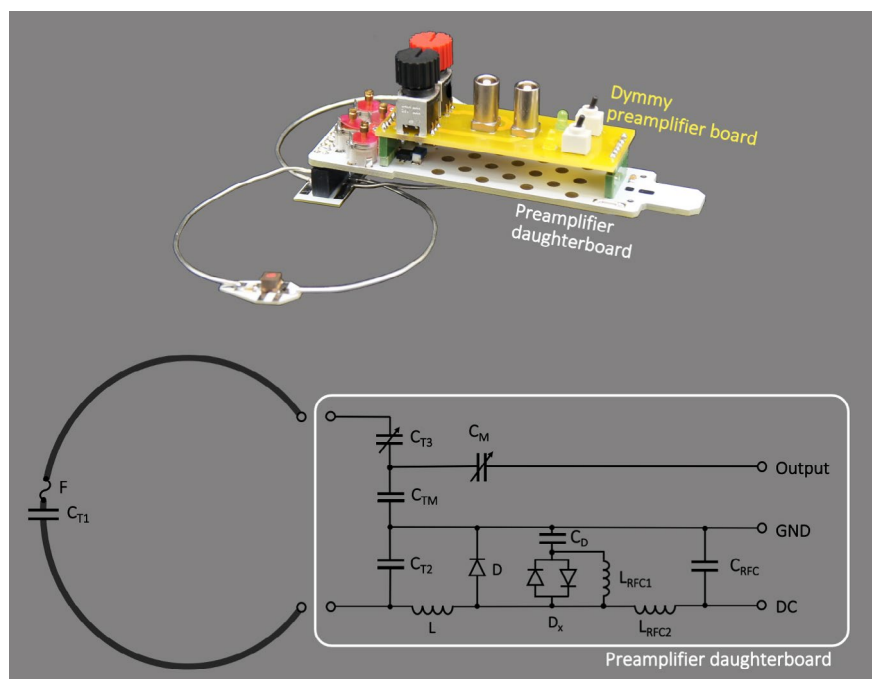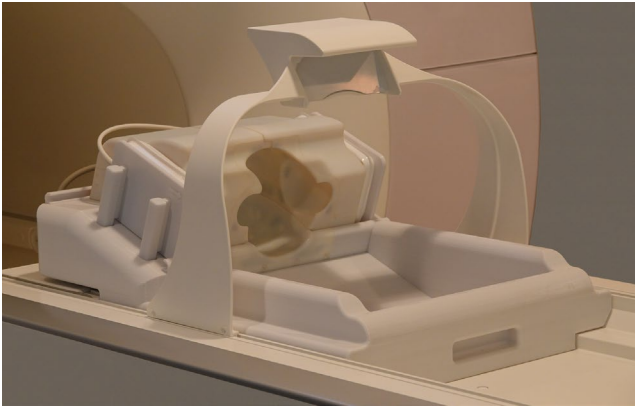
FIGURE 4 Completed infant array coil installed on the scanner's patient table. The adaptive head coil is integrated into an inclined cradle base to allow an inclined position of the infant, which ultimately improves the subject's compliance. The mirror is attached directly to the patient table and can be slid to the needed position

2.3 | Coil bench measurements

The constructed infant array was adjusted and optimized with various radiofrequency (RF) bench-level metrics using vector network analyzer equipped with a 48-channel RF switch matrix (ZNB-4 and ZN-Z84, Rohde & Schwarz GmbH & Co. KG, Munich, Germany). The unloaded-to-loaded coil quality factor ratio (Q_U/Q_L) of one representative 65-mm diameter coil element was assessed within the populated but detuned array assembly using the S_{21} double-probe method.[15] After populating the receive elements on the coil formers, the daughterboards were attached to the elements' subconnector sockets (Figure 3). All elements were pre-tuned to resonate at the Larmor frequency, and the active detuning circuitry was adjusted to switch off each element on the bench setup. We used a custom-made coil plug simulator to control each channel's detuning bias. However, the specific MRI scanner's RF architecture requires a shared bias control of 2 coil elements. Therefore, we developed a preamplifier dummy board (Figure 3), which allows the independent control of the paired coil loops. The preamplifier dummy board was designed to further provide (a) a 50 Ω termination of the loop, (b) the complex input impedance of the preamplifier, and (c) a pass-through connection for obtaining S_{11} measurement of the coil element. Each of the termination settings can be dialed in via a 3-way rotary switch. For fine adjustments, the loop under testing was brought into the tuned state, while all neighboring elements were actively detuned. By performing an S_{11} measure, we tuned and matched the coil to 123.25 MHz and 50 Ω under loaded conditions. Active detuning was adjusted by carefully controlling the variable inductance L of the active detuning circuit under a S_{21} double-probe measurement. Preamplifier decoupling was monitored with the same S_{21} measure, while the loops were terminated with the complex input impedance, emulated by the preamplifier dummy board. Small adjustment offsets of preamplifier decoupling were compensated by slightly varying the series matching capacitor C_M. Finally, all cable traps were tuned to block currents at Larmor frequency using a pair of custom-made current probes via S_{21} measurements.

2.4 | MRI acquisition and reconstruction

Initial imaging of the constructed infant array coil was carried out with a 3 Tesla MRI Scanner (MAGNETOM, Prisma, Siemens Healthineers AG, Erlangen, Germany). We used phantom imaging to determine the safety parameters, SNR, and acceleration capability metrics. Three size-matched infant head phantoms were filled with agarose and dielectrically tuned with NaCl (0.5%) and NiCl$_2$ (2.82 g/1 L H$_2$O) to match the human average brain tissue at 3 T. The dielectric values were measured to be $\sigma = 0.63$ S/m and $\epsilon_r = 78$ (DAK-12, Schmid & Partner Engineering AG, Zurich, Switzerland).

Initial infant in vivo images were collected in a sleep study and an awake task-based fMRI study. Proton density-weighted gradient-echo images obtained from phantom scans were acquired to compute the signal-to-noise ratio (SNR), g-factor, and noise correlations (repetition time TR = 30 ms, echo time TE = 6 ms, flip angle FA = 15°, slice thickness SL = 4 mm, number of slices nSL = 20, matrix M = 128 × 128, field-of-view FOV = (160 × 160) mm^2, bandwidth BW = 200 Hz/pixel, number of averages AVG = 4). The noise correlation was derived by the same sequence, where no RF excitation pulse was applied. The SNR maps were calculated for images combined from noise-covariance weighted root sum-of-squares (cov-RSS) of the individual channel images, where the weights utilize coil sensitivity maps and noise covariance information.[14,16] We computed the SENSE g-factor maps[17] for simultaneous multislice (SMS) imaging.[18,19] The maximum g-factor was determined after applying a 5 × 5 pixel sliding window filter to the g-factor maps to avoid biasing the maximum g-factor by noise singularities. These measurements were compared to a commercially available 32-channel adult head coil.

Prior to in vivo infant imaging, we performed a battery of service scans to assess coil safety for human use.[10,20] In brief, potential RF heating was measured (Fluke 61 IR Thermometer, Fluke, Everett, WA, USA) by increasing the RF power above 200% SAR, where the detuned coil and phantom were scanned for 15 minutes within a 30 μT B_1-field with a body coil's duty cycle of 10%. Potential gradient heating was assessed with ultrafast gradient readouts to induce eddy current heating from the gradient switching. For both RF and gradient heating tests, the safety watchdog was switched off for SAR and gradient stimulation, respectively. The infant coil was considered to be safety validated when the local temperature increase was under 2°C.

In vivo infant imaging was performed under the approved institutional review board (IRB) protocol at the Massachusetts Institute of Technology. Initial infant brain imaging was carried out in 2 fMRI studies with sleeping and awake infants (Figure 5). In the sleeping fMRI study, 38 infants participated, ranging from 2.0 to 11.9 weeks of age. For comparison with the adult coil, 15 infants were scanned using the constructed infant array coil, and 23 infants were scanned with the 32-channel adult head coil. Infants had adequate hearing protection, consisting of thin-layered sticky mini-muffs (first layer) surrounded by plastic shell muffs (second layer). Within hearing protection, we integrated infant-specific, MR-compatible headphones (Sensimetrics Corp., Gloucester, MA). Acoustic attenuation levels were measured using a sound meter (Svantek 979, SVANTEK Sp zo.o., Warsaw, Poland) attached to a microphone (GRAS 46AO 1/2" CCP Pressure Standard Microphone Set, GRAS Sound ″ Vibration, Holte , Denmark) with an ear and cheek simulator (GEAS 43AG, Holte , GRAS Sound & Vibration Denmark).

During the fMRI acquisitions, the sleeping infants perceived auditory stimuli, where they listened to 4 different

FIGURE 5 Infant in constructed 32-channel array coil. MR-safe infant-specific headphones were applied to the infant, and infants were placed comfortably in a cradle-shaped bassinet (A). Anterior coils accommodate headphones, close comfortably around the infant's head, and are held in place by inflatable pillows (B)

sound conditions played at 75 dB. Infants listened to 72 seconds of auditory stimulation followed by 18 seconds of silence for as long as the infant was asleep, but no longer than 30 minutes. For the fMRI acquisition, we used an echo planar imaging (EPI) sequence (TR = 2 seconds, TE = 30 ms, FA = 90°, SL = 2 mm, slice gap = 0 mm, 52 near-axial slices, M = 104 × 104, FOV = (208 × 208) mm^2, SMS multiband (MB) factor = 2) and for a structural scan, we used a motion-corrected, 3D anatomical, vNav-MPRAGE sequence[21-23] (TR = 2520 ms, 4 echoes with echo time TE_1 = 1.69 ms, TE_2 = 3.55 ms, TE_3 = 5.41 ms, TE_4 = 7.27 ms echoes combined with the root mean square, FA = 7°, SL = 1 mm, 144 near-axial slices, M = 160 × 160 × 144, FOV = (160 × 160 × 144) mm^3). We analyzed the rigid body motion parameters (translation and rotation movement) from the BOLD-EPI images obtained from both head coils. First, we computed the number of volumes that were greater than 3 different thresholds (0.5, 1.0, or 2.0 mm translation or degrees of rotation). The total number of high-motion volumes for each threshold was divided by the total number of volumes to create a single number, reflecting the percentage of high-motion volumes for each subject. The percentage of high-motion volumes was averaged across subjects for each threshold.

In the awake fMRI study, 43 infants (3-9 months old) were scanned while watching videos of faces, bodies, objects, and scenes. EPI data were collected with 44 near-axial slices (TR = 3 s, TE = 30 ms, FA = 90°, SL = 2 mm, slice gap = 0 mm, M = 80 × 80, FOV = (160 × 160) mm^2). We also collected data from 2 infants with the same acquisition sequence used in the sleeping study (TR = 2 s, TE = 30 ms, FA = 90°, SL = 2 mm, slice gap = 0 mm, 52 near-axial slices, M = 104 × 104, FOV = (208 × 208) mm^2, MB = 2). Functional data were skull-stripped (FSL BET2), registered, intensity normalized, and spatially smoothed with a 33 mm full width at half maximum (FWHM) Gaussian kernel (FSL SUSAN). High motion volumes (< 0.5° rotation or 0.5 mm rotation) were scrubbed prior to data analysis. Functional data were analyzed according to our previous study.[5] In brief, a whole-brain voxel-wise general linear model (GLM) was used with custom MATLAB scripts (R2019b, The Mathworks Inc., Natick, MA). The GLM included 4 condition regressors, 6 motion regressors, a linear trend regressor, and 5 principal component analysis (PCA) noise regressors. Condition regressors were defined as a boxcar function for the duration of the stimulus presentation. Infant inattention or sleep was accounted for using a single impulse nuisance regressor, which was defined as a boxcar function with a 1 for each TR. In case the infant was not looking at the stimuli, the condition boxcar function for the corresponding TR was changed to 0 for all condition regressors. Boxcar condition and sleep regressors were convolved with an infant hemodynamic response function (HRF) characterized by a longer time to peak

and a deeper undershoot compared with the standard adult HRF.[24] PCA noise regressors were computed using a method similar to GLMDenoise,[25] as defined by Deen et al.[5] Using in-house MATLAB scripts, one-subject-level contrast maps were computed as the difference between faces and scenes and a second as the difference between faces and objects.

3 | RESULTS

The majority of the 32 coil elements comprised a loop with a diameter of 65 mm, which showed a $Q_{UL}/Q_L = 4.3$ when surrounded by the 6 non-resonating neighboring elements. Thus, the constructed loops are sample noise dominated. Upon sample loading, a resonance frequency shift of -0.3 MHz was measured. For the 2 larger eye loops (elliptical shaped, $d_1 = 85$ mm and $d_2 = 91$ mm), we measured an unloaded-to-loaded Q-ratio of 8.6 and a loading frequency shift of -0.6 MHz.

The impedance matching to 50 Ω of the coil elements remained nearly constant due to the adjustability of the coil array to different size infant head phantoms. Only the smallest head phantom, which corresponds to newborns, had a small space between the coil former and phantom, resulting in a slightly underloaded matching condition (-22 dB).

The decoupling between the tuned and active detuned states provided an average isolation of (43 ± 2) dB. The interelement coupling is shown in Supporting Information Figure S5 as an S-matrix. Adjacent pairs of loops showed an average geometrical decoupling of $-(15 \pm 3)$ dB. The

decoupling of the next nearest neighbors ranged from -58.4 to -13.2 dB with a mean value of -28.9 dB. All decoupling values were further reduced by (17 ± 2) dB via preamplifier decoupling. The decoupling measurements were obtained when the adaptable array coil segments were positioned for their smallest sample size (default position). Cable trap tuning was measured with a set of current probes and yielded 41 dB RF current suppression at Larmor frequency.

Figure 6 shows the comparison of SNR maps between the constructed infant head coil and the commercially available adult head coil obtained from unaccelerated images, which were combined with the covariance weighted root sum-of-square (cov-RSS) reconstruction method. Both coils were loaded with an infant head phantom filled with agarose. We measured a 2.7-fold increase in SNR in the phantom region corresponding to the infant's brain. The peripheral and central regions of the brain phantom showed 3-fold and 1.25-fold SNR gains, respectively, when the constructed coil was compared with the adult coil. The SNR comparison between 3 different coil adjustment settings with its corresponding head phantoms is shown in Supporting Information Figure S1.

The noise correlation information for both when the array coil is in its default position and when the lateral coil segments are not fully closed (for larger head sizes) are shown in Figure 7. In the default position, the noise correlation ranged from 0.2% to 38.5% with an average of 11.3%. When the coil housing was adjusted for larger head sizes, we measured an average noise correlation of 9.1% (range from 0.1% to 44.8%). In comparison, when the small infant head phantom was
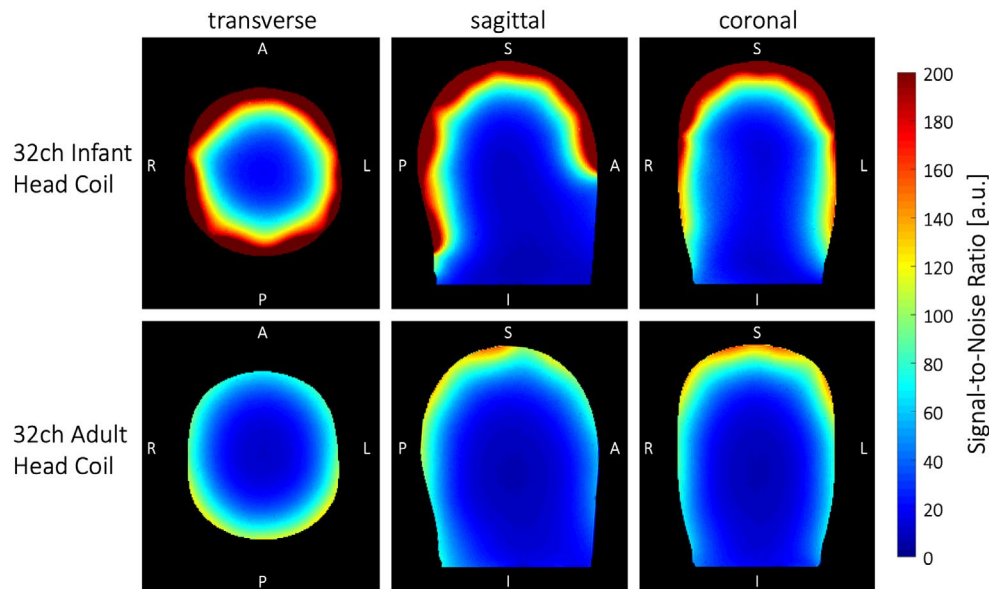

FIGURE 6 SNR comparison between the constructed 32-channel infant head coil and the commercial 32-channel adult head coil obtained from unaccelerated phantom images combined with the cov-RSS reconstruction method. The infant coil array shows a 2.7-fold SNR increase across the whole brain region in comparison to the adult head coil. In the peripheral and central regions, the infant coil outperforms the adult coil by 3-fold and 1.25-fold SNR gains, respectively
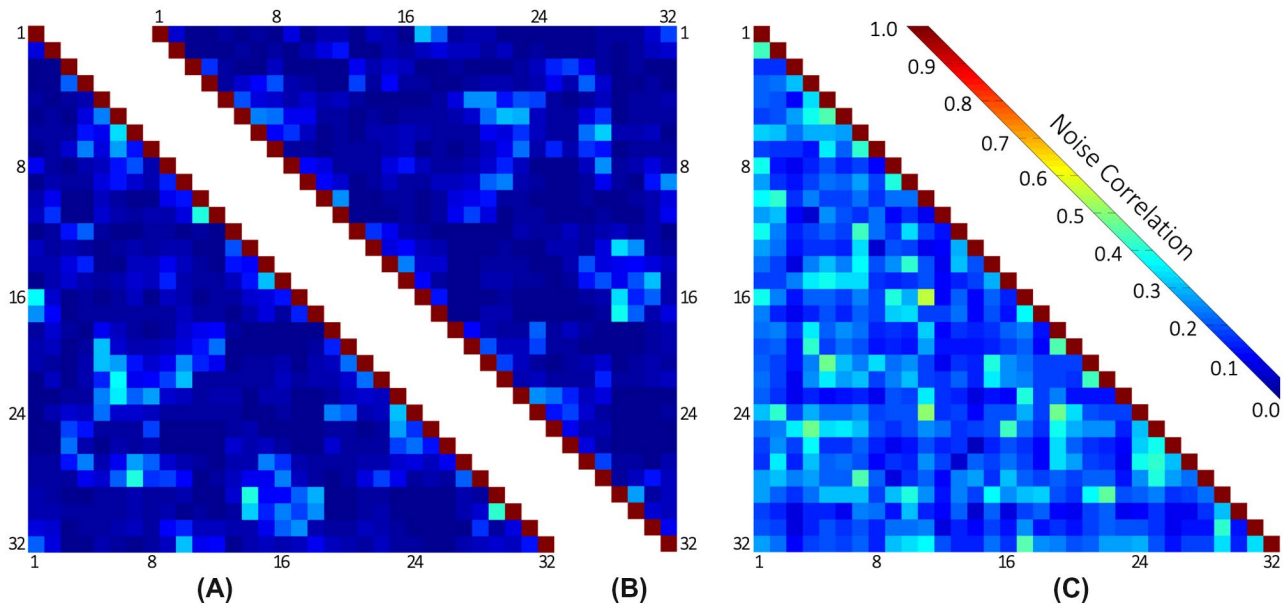
FIGURE 7 Noise correlation comparison between the infant array (A) when it is in its default position (smallest adaptive size), (B) when it is adjusted for larger head sizes, and (C) when the infant head phantom is placed in the adult head array coil. The average off-diagonal matrix elements for (A), (B), and (C) are 11.3 % (range 0.2 %-38.5 %), 9.1 % (range 0.1 %-44.8 %), and 21.6 % (range 6.3 %-61.4 %), respectively

placed in the adult head coil, a highly increased average noise correlation of 21.6 % was observed (range from 6.3 % to 61.4 %).

Since modern neuroimaging takes advantage of the recently introduced accelerated SMS imaging technique, we particularly evaluated the array coil's encoding characteristics for multislice acquisitions (Figure 8). For an acceleration MB factor of 6, the 32-channel infant coil showed almost no noise amplification during the SMS reconstruction method (max. g_{max}-factor across 6 slices = 1.06), where the 32-channel adult coil showed a maximum SMS g_{max}-factor of 1.22. When SMS is combined with in-plane undersampled k-space acceleration techniques, acceleration factors of $MB = 4$ and $R = 2$ are feasible. Here, we measured a peak noise amplification of $g_{max} = 1.2$ and $g_{max} = 2.5$ with the infant coil and with the adult coil, respectively.

The 32-channel infant array coil passed all safety tests. The amount of power from the RF body coil dissipated in the detuned array was less than 5 %. Component heating obtained from high duty cycle RF fields and eddy currents were measured to be less than 2 °C.

The hearing protection attenuated 19.8 dB at 500 Hz, 23.3 dB at 1 kHz, 26.8 dB at 4 kHz, and 28.1 dB at 10 kHz. Thus, passing the heating and sound level tests, the 32-channel infant coil was approved for in vivo infant MRI measurements.

Figure 9 shows the comparison of infant head motion using the 32-channel adult coil and the 32-channel constructed infant coil during the sleeping auditory fMRI study. Infants placed in the dedicated adaptive head coil showed substantial lower head motion when compared with the adult coil. When the infants fell asleep, we collected enough data

for data analysis (≥ 90TRs) from 91% of infants in the adult coil and 100% of infants in the infant coil.

Figure 10 shows preliminary data from a single awake infant (6 months old) with 13.5 minutes of low-motion data on the 2 following canonical contrasts: faces > scenes and faces > objects. The high-resolution EPI images obtained from the infant array coil enabled the acquisition of high-quality functional data of an awake infant performing a task-based study. Of the 43 infants who were recruited for the awake study, we collected enough low-motion data (< 0.5° rotation or 0.5 mm rotation) for analysis (≥ 95TRs) from 23 out of 43 infants (53%).

4 | DISCUSSION

In this study, we designed, constructed, and evaluated a size-adaptive 32-channel infant head coil, which was especially developed for scanning awake infants. The coil was compared to a commercially available adult head coil and evaluated with bench tests and phantom imaging. Although 32-channel head array coils are well understood at 3 T,[10,20,26-30] there are additional challenges when using the concept of an adaptable head coil design for awake infants. Several design considerations had to be addressed for a functional coil former when imaging this young population. First, a convenient segmentation of the coil former needed to be implemented. To provide easy coil handling while the infant is placed inside the head coil, we subdivided the coil former into 3 segments. The posterior coil part is anatomically shaped to adapt to the occipital lobe of the infant's head, while the 2 anterior housing
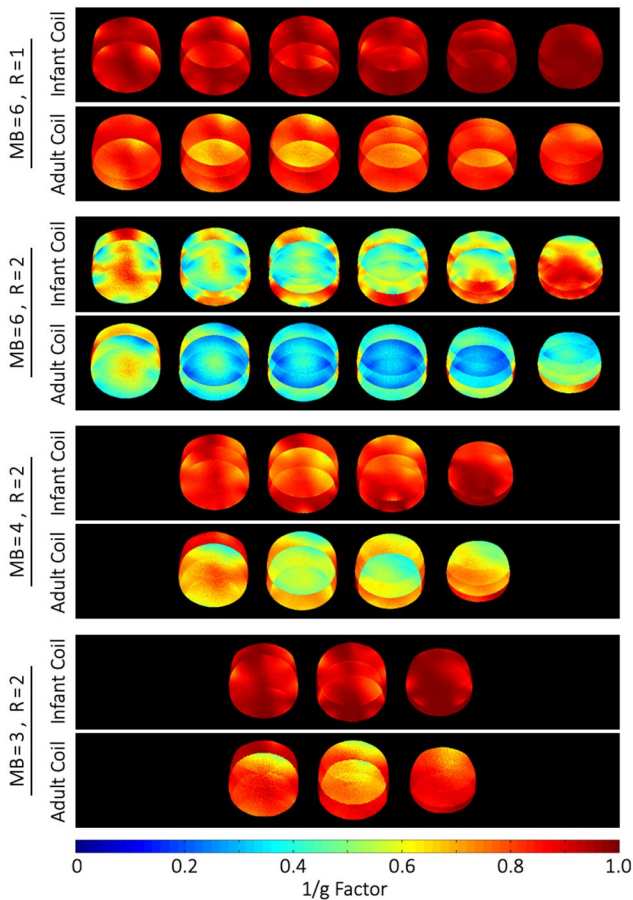
FIGURE 8 Comparison of accelerated image encoding capabilities when using simultaneous multislice (SMS) reconstruction techniques. The constructed infant head coil shows substantially lower noise amplification during SMS or combined SMS/in-plane acceleration

FIGURE 9 Subject volume-to-volume motion in 32-channel adult and 32-channel infant coils. Infants participated in a sleeping auditory fMRI study. Headphones were applied, and infants were placed in either a standard 32-channel adult coil ($n = 23$) or the 32-channel infant coil ($n = 15$). Data were collected using the same EPI, and volume-to-volume motion (mm of translation and degrees of rotation) was calculated. Infants scanned with the adult coil had a higher average percentage of volumes that exceeded motion thresholds at 0.5 mm (mean = 9.5, s.e.m. = 3.8), 1.0 mm (mean = 7.1, s.e.m. = 3.6), and 2.0 mm (mean = 4.5, s.e.m. = 2.2) than the infant coil at 0.5 mm (mean = 4.7, s.e.m. = 1.1), 1.0 mm (mean = 3.1, s.e.m. = 0.7), and 2.0 mm (mean = 1.9, s.e.m. = 0.5)

parts are laterally adjustable. This 3-segment design provides a compromise between a high degree of geometrical adaptability, and it greatly simplifies the handling of the coil setup on the scanner's patient table.

Maintaining a tight fit of the 32 channels around the subject's head is critical in gaining SNR. However, it potentially limits the usage of proper ear protection. Therefore, we needed to rethink how to incorporate the ear protection gear into the helmet. By implementing compartments in the lateral housing parts, we could maintain a snug fit of the coil and simultaneously ensure appropriate sound protection by using thin-layered mini-muffs and additional plastic shell muffs. In total, we obtained a reduction of acoustic noise ranging from 19.8 dB (500 Hz) to 28.1 dB (10 kHz) for the MRI relevant acoustic frequencies. The inflatable cushions have proven valuable for firmly sealing the earmuffs and achieving a close fitting of the array coil. For accomplishing higher completion rates of infant MRI scans, a critical design component was the incorporation of an inclined cradle seat. In this position, the infant can maintain eye contact with parents during the setup process on the patient's table. According to our infant
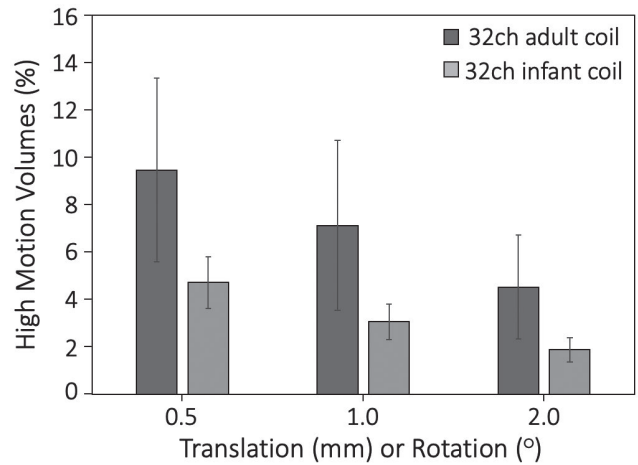
MRI scan experiences obtained from initial studies, the infant favors the inclined position over the regular supine position, which is typically used during adult MRI brain examinations. In general, this position of the infant is similar to that in a car seat, which infants and toddlers are already used to.

When a head coil former is subdivided into multiple segments and employs 32 small receive loop elements, several technical issues need to be addressed. Distributing the loops while maintaining the geometrically overlapped regions across coil former segments becomes more difficult. The mechanical implementation of the housing splits was accomplished by a rim structure allowing neighboring loop elements of adjacent coil former segments to overlap. Consequently, the geometrically given constraints forced many loop elements within the array to be non-circular and to bend over the housing's rim structure.

The capability of the array to adapt to different head sizes changes the critical overlap in the region of the housing splits. While the geometrical overlap was optimized at the default housing position (smallest head size), the critical overlap could clearly not be maintained when the array coil was adjusted for larger head sizes. This yielded a slight increase of coil coupling between adjacent loops across the housing segments, which could be seen in a noise correlation rise of approximately 6 dB for affected loop pairs. The established preamplifier decoupling of 17 dB provides enough overhead to prevent the negative impact of losing the coil's load impedance of 50 Ω because

FIGURE 10 Comparison of 2 canonical contrast faces > scenes (top) and faces > objects (bottom) in an example subject. Data were collected using EPI sequence with $MB = 2$ from an awake 6-month-old infant watching colorful videos of faces, bodies, objects, and scenes. After motion scrubbing, 13.5 minutes of data were available for inclusion in the analysis. Face activation (red) is in the same areas for both the contrast of faces > scenes (top) and faces > objects (bottom). Similar data were collected from other subjects
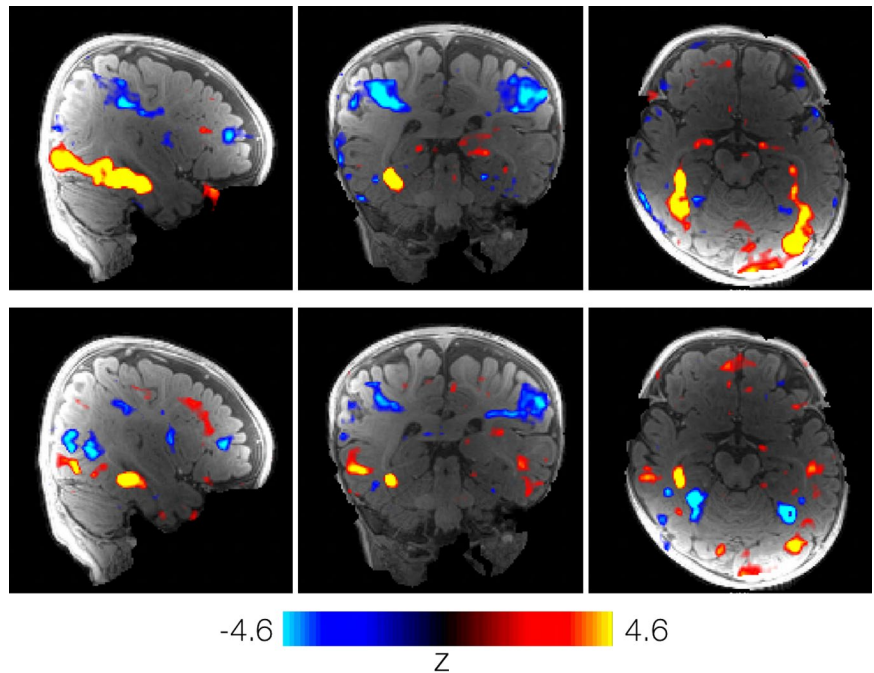
of the changed and increased mutual inductive coupling. Thus, it is still possible to maintain the critical load impedance to drive the preamplifier with its lowest noise figure. The slightly increased coupling can then be compensated by incorporating the noise covariance statistics in the image combination algorithm. Interestingly, while observing a higher noise correlation of the cross housing adjacent loop pairs, the average noise correlation decreased by 2.2% when the coil setup was adjusted for larger head sizes. This can potentially be attributed to the overall larger geometrical distance between coil elements within the housing subdivisions.

However, when placing a relatively small head size into the adult head coil, the small head size significantly underloads the coil array. This negatively affects the matching of the coil elements, which yields a suboptimal noise figure of the preamplifier's performance. Furthermore, the underloaded condition increases the Q-factor of the adult coil's elements, which causes increased intercoil element coupling. This can be seen in an elevated level of the average noise correlation.

As we have shown in previous pediatric brain studies,[5,10,31,32] a dedicatedly designed tight-fitting array coil for the pediatric population provides substantial SNR benefits over adult head coils. Our constructed adjustable array coil shows similar results. On average, the infant coil outperforms the adult head coil by a factor of 2.7 of SNR gain in the brain region. The improved SNR can be invested into smaller voxel sizes, providing MR brain images with higher resolution. Furthermore, the loss of critical coil overlap between the split segments of the expanded array did not negatively impact the overall SNR performance, indicating that the pre-whitening process of the cov-RSS image reconstruction method compensated well for the increased couplings. In the widest coil

helmet setting, the small gap between the segments slightly modulated the SNR pattern at the periphery of the phantom. However, small gaps between loop elements are not considered critical in array coils, as can be seen in a very common head coil design, the gapped-array design.[33]

The enhanced performance in parallel imaging encoding can be attributed to the smaller loop sizes and to the close-fitting array. In particular, this improves the steepness of the sensitivity profiles (eg, SENSE) in the signal given area or the synthesis of the spatial harmonics for k-space-based reconstruction techniques (eg, GRAPPA). The literature clearly shows g-factor improvements by employing a higher channel count. However, in infant brain imaging, we can achieve similar improvements by reducing the overall loop diameters while keeping the channel count unaltered.

Recently, SMS imaging has been introduced to accelerate image acquisitions with minimal penalty of SNR loss. In advanced functional neuroimaging, the SMS technique is combined with regular in-plane parallel imaging methods to take advantage of the shortened echo train to minimize image distortion during EPI fMRI scans. Hence, our constructed infant coil was optimized to provide sufficient encoding power in both slice direction and 2-dimensional in-plane directions. The SMS g-factor maps show substantial improvements using the infant array coil when compared with the adult head coil. Thus, the developed coil is well-suited to accelerate image encoding and to shorten overall image acquisition time, which has proven critical to increase the completion rate when performing MR infant neuroimaging.

Imaging the pediatric population in both clinical and research settings remains a challenging undertaking because of methodological requirements. One of the biggest constraints

in completing a pediatric fMRI scan is associated with motion artifacts. Due to mechanical advances, the developed infant coil setup increased infants' comfort with the inclined position and reduced the range of allowable head motion. However, for further improvement of motion restriction during fMRI scans, prospective motion compensation techniques can be combined with our developed infant array coil. Currently established motion correction techniques, which show promising results, use optical methods to detect the subject's head movement. Since we designed the coil with an open-faced topology, it could potentially facilitate optical prospective motion compensation methods.

5 | CONCLUSIONS

By optimizing the shape and functionality of an infant brain array coil to allow head size adaptability, high-level sound protection, and head motion restriction, we improved infant brain MRI in terms of sensitivity, spatial resolution, and accelerated encoding capabilities. Furthermore, we changed the paradigm of imaging infants from a flat supine position to a half-seated position; combined with the coil's integrated ear protection, this increased the subject's tolerance for undergoing MRI neuroexaminations. We could demonstrate SNR gains, fast image encoding power, and improved scan completion rates by capitalizing on technical advances for both coil array technology and mechanical features that were tailored to the infant population.

ORCID
Anpreet Ghotra http://orcid.org/0000-0001-6445-9062
Heather L. Kosakowski http://orcid.org/0000-0001-5689-0426
Atsushi Takahashi http://orcid.org/0000-0002-5182-4320
Robin Etzel http://orcid.org/0000-0002-8783-589X
Markus W. May https://orcid.org/0000-0003-3869-9681
Alina Scholz https://orcid.org/0000-0002-3324-6889
Lawrence L. Wald http://orcid.org/0000-0001-8278-6307
Nancy Kanwisher http://orcid.org/0000-0003-3853-7885
Boris Keil http://orcid.org/0000-0003-0805-8330

REFERENCES
1. Konishi Y, Taga G, Yamada H, Hirasawa K. Functional brain imaging using fMRI and optical topography in infancy. *Sleep Med*. 2002;3(Suppl 2):S41-S43.
2. Dinstein I, Pierce K, Eyler L, Solso S, Malach R, Behrmann M, Courchesne E. Disrupted neural synchronization in toddlers with autism. *Neuron*. 2011;70:1218-1225.
3. Damaraju E, Caprihan A, Lowe JR, Allen EA, Calhoun VD, Phillips JP. Functional connectivity in the developing brain: a longitudinal study from 4 to 9 months of Age. *Neuroimage*. 2014;84:169-180.
4. Hughes EJ, Winchman T, Padormo F, Teixeira R, Wurie J, Sharma M, Fox M, Hutter J, Cordero-Grande L, Price AN, Allsop J, Bueno-Conde J, et al. A dedicated neonatal brain imaging system. *Magn Reson Med*. 2017;78:794-804.
5. Deen B, Richardson H, Dilks DD, Takahashi A, Keil B, Wald LL, Kanwisher N, Saxe R. Organization of High-Level Visual Cortex in Human Infants. *Nat Commun*. 2017;8:13995.
6. Ellis CT, Skalaban LJ, Yates TS, Bejjanki VR, Córdova NI, Turk-Browne NB. Re-imagining fMRI for awake behaving infants. *Nat Commun*. 2020;11:4523.
7. Gilmore JH, Shi F, Woolson SL, Knickmeyer RC, Short SJ, Lin W, Zhu H, Hamer RM, Styner M, Shen D. Longitudinal development of cortical and subcortical gray matter from birth to 2 years. *Cereb Cortex*. 2012;22:2478-2485.
8. WHO. *The WHO Child Growth Standards*. https://www.who.int/tools/child-growth-standards/standards/head-circumference-for-age. Accessed April 1, 2005.
9. Poduslo SE, Jang Y. Myelin development in infant brain. *Neurochem Res*. 1984;9:1615-1626.
10. Keil B, Alagappan V, Mareyam A, McNab JA, Fujimoto K, Tountcheva V, Triantafyllou C, Dilks DD, Kanwisher N, Lin W, Grant PE, Wald LL. Size-Optimized 32-channel brain arrays for 3 T pediatric imaging. *Magn Reson Med*. 2011;66:1777-1787.
11. Rios NL, Foias A, Lodygensky G, Dehaes M, Cohen-Adad J. Size-Adaptable 13-channel receive array for brain MRI in human neonates at 3 T. *NMR in Biomedicine*. 2018;31:e3944.
12. Nellhaus G. Head circumference from birth to eighteen years. Practical composite international and interracial graphs. *Pediatrics*. 1968;41:106-114.
13. Roche AF, Mukherjee D, Guo SM, Moore WM. Head circumference reference data: birth to 18 years. *Pediatrics*. 1987;79:706-712.
14. Roemer PB, Edelstein WA, Hayes CE, Souza SP, Mueller OM. The NMR phased array. *Magn Reson Med*. 1990;16:192-225.
15. Hoult DI, The NMR. Receiver: a description and analysis of design. *Prog Nucl Magn Reson Spectrosc*. 1978;12:41-77.
16. Kellman P, McVeigh ER. Image reconstruction in SNR units: a general method for SNR measurement. *Magn Reson Med*. 2005;54:1439-1447.
17. Pruessmann KP, Weiger M, Scheidegger MB, Boesiger P. SENSE: sensitivity encoding for fast MRI. *Magn Reson Med*. 1999;42:952-962.
18. Setsompop K, Gagoski BA, Polimeni JR, Witzel T, Wedeen VJ, Wald LL. Blipped-Controlled Aliasing in Parallel Imaging for Simultaneous Multislice Echo Planar Imaging with Reduced g-Factor Penalty. *Magn Reson Med*. 2012;67:1210-1224.
19. Feinberg DA, Moeller S, Smith SM, Auerbach E, Ramanna S, Gunther M, Glasser MF, Miller KL, Ugurbil K, Yacoub E. Multiplexed echo planar imaging for sub-second whole brain FMRI and fast diffusion imaging. *PLoS ONE*. 2010;5:e15710.
20. Keil B, Blau JN, Biber S, Hoecht P, Tountcheva V, Setsompop K, Triantafyllou C, Wald LL. A 64-channel 3T array coil for accelerated brain MRI. *Magn Reson Med*. 2013;70:248-258.
21. van der Kouwe AJW, Benner T, Salat DH, Fischl B. Brain morphometry with multiecho MPRAGE. *Neuroimage*. 2008;40:559-569.
22. Tisdall MD, Hess AT, Reuter M, Meintjes EM, Fischl B, van der Kouwe AJW. Volumetric vavigators (vNavs) for prospective motion correction and selective reacquisition in neuroanatomical MRI. *Magn Reson Med*. 2012;68:389-399.

23. Tisdall MD, Reuter M, Qureshi A, Buckner RL, Fischl B, van der Kouwe AJW. Prospective motion correction with volumetric navigators (vNavs) reduces the bias and variance in brain morphometry induced by subject motion. *Neuroimage*. 2016;127:11-22.

24. Arichi T, Fagiolo G, Varela M, Melendez-Calderon A, Allievi A, Merchant N, Tusor N, Counsell SJ, Burdet E, Beckmann CF, Edwards AD. Development of BOLD signal hemodynamic responses in the human brain. *Neuroimage*. 2012;63:663-673.

25. Kay KN, Rokem A, Winawer J, Dougherty RF, Wandell BA. GLMdenoise: a fast, automated technique for denoising task-based fMRI data. *Front Neurosci*. 2013;7:247.

26. Keil B, Wald LL. Massively parallel MRI detector arrays. *J Magn Reson*. 2013;229:75-89.

27. Farivar R, Grigorov F, van der Kouwe AJ, Wald LL, Keil B. Dense, Shape-Optimized Posterior 32-Channel Coil for Submillimeter Functional Imaging of Visual Cortex at 3T. *Magn Reson Med*. 2016;76:321-328.

28. Chu YH, Hsu YC, Keil B, Kuo WJ, Lin FH. A 32-channel head coil array with circularly symmetric geometry for accelerated human brain imaging. *PLoS One*. 2016;11.

29. Wiggins GC, Triantafyllou C, Potthast A, Reykowski A, Nittka M, Wald LL. 32-channel 3 Tesla receive-only phased-array head coil with soccer-ball element geometry. *Magn Reson Med*. 2006;56:216-223.

30. Lattanzi R, Grant AK, Polimeni JR, Ohliger MA, Wiggins GC, Wald LL, Sodickson DK. Performance evaluation of a 32-element head array with respect to the ultimate intrinsic SNR. *NMR Biomed*. 2010;23:142-151.

31. Cohen MA, Dilks DD, Koldewyn K, Weigelt S, Feather J, Kell AJ, Keil B, Fischl B, Zöllei L, Wald L, Saxe R, Kanwisher N. Representational similarity precedes category selectivity in the developing ventral visual pathway. *Neuroimage*. 2019;197:565-574.

32. Richardson H, Gweon H, Dodell-Feder D, Malloy C, Pelton H, Keil B, Kanwisher N, Saxe R. Response patterns in the developing social brain are organized by social and emotion features and disrupted in children diagnosed with autism spectrum disorder. *Cortex*. 2020;125:12-29.

33. Ledden PJ, Mareyam A, Wang S, van Gelderen P, Duyn J. 32-channel receive-only SENSE array for brain imaging at 7T. In Proceedings of the International Society for Magnetic Resonance in Medicine, Berlin, Germany, 2007. #242.

34. Keil B. *Github Repository*. 2021. https://github.com/keyarray/infantmricoil.

SUPPORTING INFORMATION

Additional Supporting Information may be found online in the Supporting Information section.

FIGURE S1 Adjustment mechanism for infant head sizes and corresponding SNR comparison. A, For newborns up to 2 months, the coil is not entirely filled and a small space of 1-1.5 cm remains between the head and the coil former. In this case, the coil is in the narrowest helmet setting. B, In the same coil setting, the coil can accommodate infants with a head circumference of up to 44 cm (equivalent to 6-8 months). C, For larger head sizes, the coil former allows expansion in the left-right and anterior-posterior directions, essentially losing the critical overlap of adjacent loops across the housing segments

and causing small gaps. The latter slightly modulates the SNR pattern at these specific locations on the periphery of the phantom. D, The 3 representative head sizes of a, b, and c are positioned at the center of the 32-channel adult coil for direct dimensional comparison. The exact dimensions of the adult coil housing were obtained from a CT scan and re-drawn in the CAD program

FIGURE S2 Adaptability of the 32-channel infant coil in the anterior-posterior direction. In the standard helmet position (tightest fit), the array coil provides 155 mm of anterior-posterior length (A). The coil segments can optionally also run on top of the rails at the back (B) or at the front (C). This allows an increase in helmet size of 5 and 10 mm, respectively. When the coil segments are placed on top of both rail structures, the helmet size can be increased by a maximum of 15 mm. This setup allows head circumferences of up to 49 cm to be accommodated

FIGURE S3 Loop configuration of the constructed infant 32-channel coil array. The posterior coil former segment consists of 12 loop elements (pink). Each lateral segments (blue and green) comprise 10 loop coils

FIGURE S4 Impedance transformation circuitry for a representative loop element with 65 mm diameter. The resonance is set to Larmor with $C_{T1} = 8.7\,\text{pF}$, $C_{T2} = 56\,\text{pF}$, and $C_{TM} = 36\,\text{pF}$. The coil impedance Z_c is preset by the chosen value of C_{TM} and further transformed to $Z_0 = 50\,\Omega$ with the series matching capacitor $C_M = 24\,\text{pF}$. Preamplifier decoupling is established by transforming the complex input impedance of the preamplifier $Z_p = (8 + j87)\,\Omega$ via $C_M = 24pF$ to a parallel inductance Z_l across C_{TM}. This parallel LC circuit is set to resonate at the Larmor frequency causing a high series impedance in the coil loop

FIGURE S5 S-matrix assessment of the infant 32-channel coil. The S-matrix was measured with an 48-channel RF switch matrix VNA, when the array coil was in its default position and loaded with an agar infant head phantom. The diagonal matrix elements represent the matching of each loop coil, ranging from −26.3 to −34.1 dB. The off-diagonal matrix elements show the inductive coupling between the loop coils, ranging from −58.4 to −13.2 dB with a mean of −28.9 dB. Note, the inter-element coupling was measured when each loop coil was terminated with 50 Ω using the RF switching matrix. In the actual setup, the coupling between the coils is further reduced by terminating the coil with its preamplifier which establishes the preamplifer decoupling